Two-step phase manipulation by tailoring chemical bonds results in high-performance GeSe thermoelectrics

Wenqing Yao,[1] Yihua Zhang,[1] Tu Lyu,[1] Weibo Huang,[1] Nuoxian Huang,[1] Xiang Li,[1] Chaohua Zhang,[1] Fusheng Liu,[1] Matthias Wuttig,[2,3] Yuan Yu,[2,*] Min Hong,[4,*] and Lipeng Hu[1,*]

*Correspondence: yu@physik.rwth-aachen.de (Y.Y.); min.hong@usq.edu.au (M.H.); hulipeng@szu.edu.cn (L.H.)

Received: June 20, 2023; Accepted: October 3, 2023; Published Online: October 6, 2023; https://doi.org/10.1016/j.xinn.2023.100522

GRAPHICAL ABSTRACT

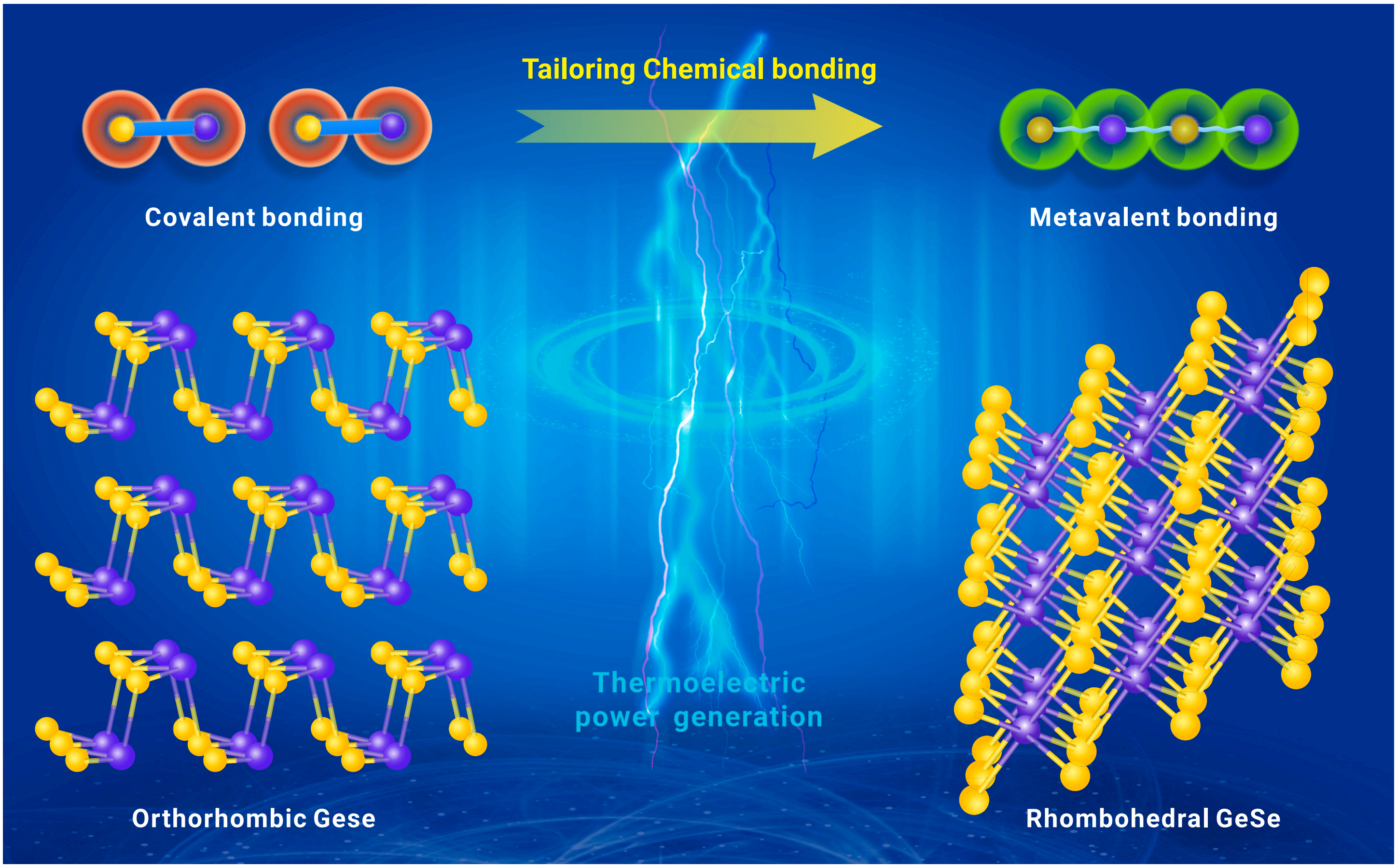

PUBLIC SUMMARY

- A two-step phase manipulation strategy by tailoring chemical bonds is proposed in GeSe.
- CdTe alloying shifts orthorhombic to rhombohedral phase and yields high valley degeneracy.
- Adding Pb restrains the Peierls distortion and triggers the valence band convergence.
- The metavalently bonded rhombohedral GeSe owns a high power factor and a low thermal conductivity.
- A high figure of merit of 0.9 is achieved in rhombohedral $Ge_{0.8}Pb_{0.2}Se(CdTe)_{0.25}$.

Two-step phase manipulation by tailoring chemical bonds results in high-performance GeSe thermoelectrics

Wenqing Yao,[1] Yihua Zhang,[1] Tu Lyu,[1] Weibo Huang,[1] Nuoxian Huang,[1] Xiang Li,[1] Chaohua Zhang,[1] Fusheng Liu,[1] Matthias Wuttig,[2,3] Yuan Yu,[2,*] Min Hong,[4,*] and Lipeng Hu[1,*]

[1]College of Materials Science and Engineering, Shenzhen University, Shenzhen 518060, China
[2]Institute of Physics (IA), RWTH Aachen University, Sommerfeldstraße 14, 52074 Aachen, Germany
[3]PGI 10 (Green IT), Forschungszentrum Jülich GmbH, 52428 Jülich, Germany
[4]Center for Future Materials and School of Engineering, University of Southern Queensland, Springfield Central, QLD 4300, Australia
*Correspondence: yu@physik.rwth-aachen.de (Y.Y.); min.hong@usq.edu.au (M.H.); hulipeng@szu.edu.cn (L.H.)

Received: June 20, 2023; Accepted: October 3, 2023; Published Online: October 6, 2023; https://doi.org/10.1016/j.xinn.2023.100522

Citation: Yao W., Zhang Y., Lyu T., et al., (2023). Two-step phase manipulation by tailoring chemical bonds results in high-performance GeSe thermoelectrics. The Innovation **4(6)**, 100522.

In thermoelectrics, phase engineering serves a crucial function in determining the power factor by affecting the band degeneracy. However, for low-symmetry compounds, the mainstream one-step phase manipulation strategy, depending solely on the valley or orbital degeneracy, is inadequate to attain a high density-of-states effective mass and exceptional zT. Here, we employ a distinctive two-step phase manipulation strategy through stepwise tailoring chemical bonds in GeSe. Initially, we amplify the valley degeneracy via CdTe alloying, which elevates the crystal symmetry from a covalently bonded orthorhombic to a metavalently bonded rhombohedral phase by significantly suppressing the Peierls distortion. Subsequently, we incorporate Pb to trigger the convergence of multivalence bands and further enhance the density-of-states effective mass by moderately restraining the Peierls distortion. Additionally, the atypical metavalent bonding in rhombohedral GeSe enables a high Ge vacancy concentration and a small band effective mass, leading to increased carrier concentration and mobility. This weak chemical bond along with strong lattice anharmonicity also reduces lattice thermal conductivity. Consequently, this unique property ensemble contributes to an outstanding zT of 0.9 at 773 K for $Ge_{0.80}Pb_{0.20}Se(CdTe)_{0.25}$. This work underscores the pivotal role of the two-step phase manipulation by stepwise tailoring of chemical bonds in improving the thermoelectric performance of p-bonded chalcogenides.

INTRODUCTION

Phase modification plays an indispensable role in materials science and engineering, as well as solid-state chemistry.[1–3] By intentionally manipulating the phases of a material, it is possible to tune its microstructure, electronic band structure, and phonon dispersion relation, which significantly influence its mechanical, physical, and chemical properties.[4–6] Therefore, the rational design and precise control of crystal structure are imperative for the development of advanced structural and functional materials. In thermoelectrics, a solid-state technology facilitating the direct conversion between heat and electricity, the crystal structure has a direct impact on the power factor, PF = $\sigma\alpha^2$, through the band degeneracy (N_V).[7–9] This, in turn, determines the material's dimensionless figure-of-merit, $zT = \alpha^2\sigma T/(\kappa_e + \kappa_L)$, where α is the Seebeck coefficient, σ is the electrical conductivity, κ_e is the carrier thermal conductivity, κ_L is the lattice thermal conductivity, and T is the absolute temperature.[10–15]

To date, phase engineering has emerged as a highly feasible strategy for achieving high PF by increasing crystal symmetry or adjusting the lattice parameters.[16–20] In general, increasing the crystal symmetry can enhance the valley degeneracy (N_V) and consequently the density-of-states effective mass (m^*).[8,21] A large m^* is beneficial to a high α at high n_H, which can simultaneously increase the σ, leading to a large PF.[22] For instance, when the crystal symmetry of $Cu_2(Te/Se/S)$ compounds shifted from monoclinic to a hexagonal structure, the m^* value greatly raised from below 2.0 m_0 to above 4.5 m_0.[23] Under a given crystal symmetry, it is conceivable to facilitate orbital convergence and elevate the m^* by tunning the lattice parameters.[24] Zhang et al. exemplified this approach by modifying the structural parameter $\eta = c/2a$ of tetragonal chalcopyrite to 1.0, achieving the coexistence of a long-range cubic framework with localized short-range non-cubic lattice distortions. This led to highly degenerate band edges and, subsequently, a larger PF.[25] Recently, a slight symmetry-breaking strategy in rhombohedral GeTe has been employed to manipulate the interaxial angle (θ) and the atomic-site displacement ($\varDelta$), triggering the convergence of multivalence bands for high TE performance.[26–29]

Nonetheless, for numerous low-symmetry compounds (eg, triclinic, monoclinic, and orthorhombic phases) with intrinsically low zT values,[7,8,23] the mainstream one-step phase manipulation strategy, which solely relies on the valley or orbital degeneracy, is insufficient to achieve a notably high m^* and, subsequently, an outstanding zT. Under such circumstances, we deduce that improving the zT value of low-symmetry materials should depend on a distinctive two-step phase manipulation strategy. The first step aims to improve the valley degeneracy by increasing the crystal symmetry, while the second step concentrates on promoting orbital convergence through further adjustment of lattice parameters for the desired crystal symmetry. However, it is still elusive how to experimentally correlate successive transitions of crystal structure and conceptualize the coined two-step phase manipulation. To accomplish this objective, a comprehensive understanding and elucidation of the pivotal factors affecting crystal structure are prerequisites. Since the atomic arrangement in a solid is a consequence of chemical bonding, tailoring chemical bonds should enable direct modification of the crystal structure and, consequently, the resulting electronic band structure.[30]

Many IV-VI chalcogenides, such as GeS, GeSe, SnS, SnSe, and GeTe, comprise various phases intrinsically interrelated with disparate chemical bonding mechanisms.[31–34] More specifically, the low-symmetric orthorhombic phase utilizes conventional covalent bonding, while the medium-symmetric rhombohedral phase and the high-symmetric cubic phase employ unique metavalent bonding (MVB).[35–37] MVB is a fundamental chemical bonding mechanism that markedly differs from textbook covalent, ionic, and metallic bonding. To be more specific, MVB describes a situation where adjacent atoms share half an electron pair (one electron) to form a σ-bond, yielding a bond order of approximately 1/2.[30] In stark contrast, a conventional covalent bond comprises two electrons shared between neighboring atoms, resulting in a bond order of 1.[38] Here, the bond order is defined as half of the difference between the number of electrons in bonding and antibonding molecular orbitals. The particular electronic configuration leads to several characteristic fingerprints in terms of material properties both related to the lattice, i.e., phonons as well as electrons in the vicinity of the Fermi level relevant for charge transport. The MVB mechanism can collapse by either increasing electron transfer or enhancing electron sharing, also known as increasing Peierls distortion (PD).[30] Conversely, reducing electron sharing, i.e., inhibiting PD, induces a gradual transition from covalent to metavalent bonding and simultaneous conversion of the crystal structure from orthorhombic to rhombohedral or even cubic structure.[30,38] Consequently, stepwise tailoring of chemical bonds is able to effectively manipulate successive phase transitions, thereby enabling continuous modification of the band structure.

In this work, p-type GeSe, as a promising TE material for medium-temperature power generation,[39–47] is selected to attest to the efficacy of two-step phase manipulation through tailoring chemical bonds. In addition, GeSe is one of the few monochalcogenides, where the wide phase space is accessible, and thus is ideal for employing and tailoring the relationship between chemical bonding and material properties. The pristine low-symmetry orthorhombic GeSe utilizing covalent bonding exhibits a poor zT of 0.05.[48] As schematically illustrated in Figure 1, alloying GeSe with CdTe substantially suppresses the PD, thereby altering the chemical bonds from covalent to metavalent and a concomitant structural

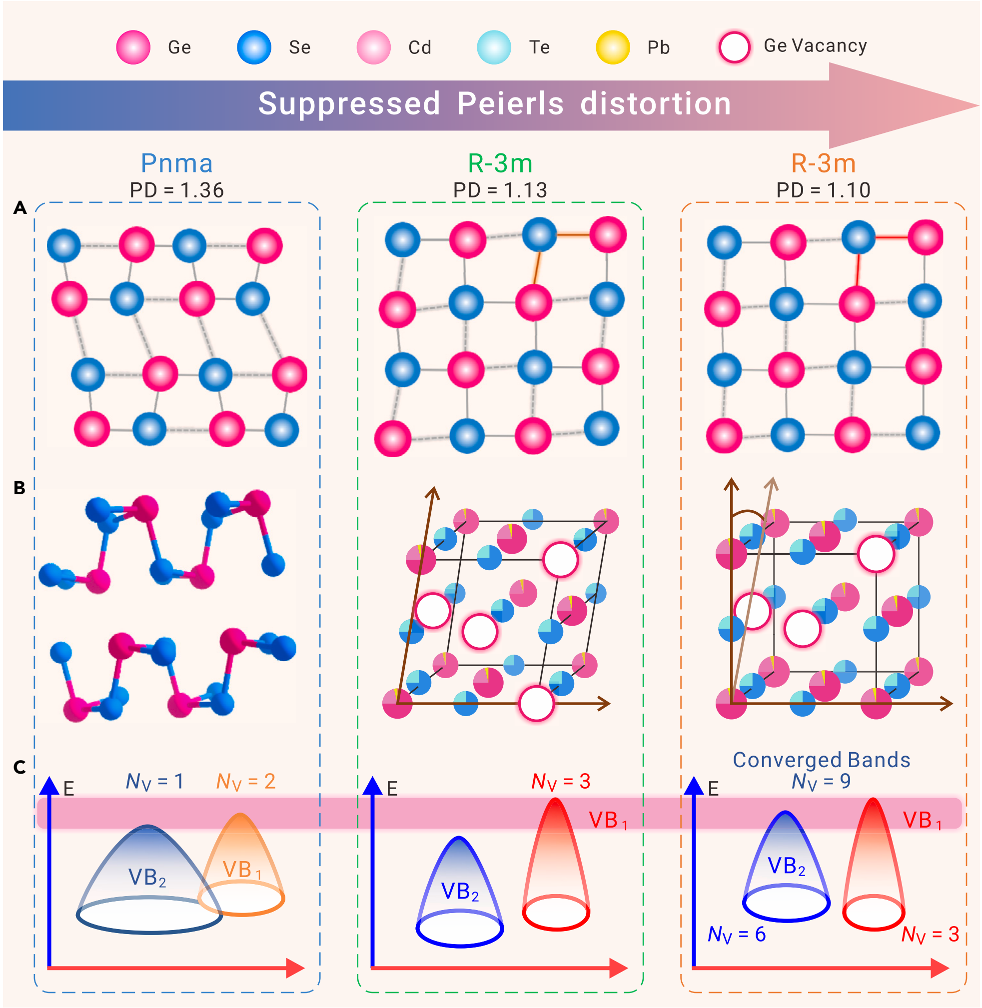

Figure 1. Schematic representation of the two-step phase manipulation through the stepwise tailoring of chemical bonds and its impact on the electronic band structures (A) Schematic representation of the variation in Peierls distortion (PD), which is the ratio between long and short bonds. The two different bond lengths are highlighted by red lines in the right schematic of (A). Note that the orthorhombic phase has two longer bonds and one short bond and thus it shows two different PD values. The larger PD = 1.36 for orthorhombic (Pnma) GeSe and the PD = 1.13 for rhombohedral (R3m) GeSe is taken from Kooi and Wuttig,[49] while the PD = 1.10 for CdTe and Pb co-alloyed rhombohedral GeSe is calculated according to the XRD refinement. (B) Schematic representation of the variation in crystal structures. (C) Schematic representation of the variation in electronic band structures. The VB_1 and VB_2 refer to the first and second valence band maximum, respectively. *E* signifies the energy level, and N_V represents the valley degeneracy of each valence band. The red-shaded region represents the vicinity of the Fermi level that dominates the charge carrier transport.

transition from a low-symmetric orthorhombic to a medium-symmetric rhombohedral phase. The enhanced crystal symmetry leads to a significant increase in valley degeneracy and thus m^*. Subsequently, we employ Pb substitution to trigger the multivalence bands convergence via slightly depressing the PD in rhombohedral GeSe(CdTe)$_x$, which further remarkably increases the N_V and m^* (Figure 1). Moreover, the reduced formation energy of Ge vacancies, smaller band gap (E_g), and lighter band effective mass (m_b^*) in metavalently bonded GeSe, compared with its covalently bonded counterpart, contribute to a higher carrier concentration (n_H) and larger carrier mobility (μ_H). Furthermore, the weaker chemical bonds and larger lattice anharmonicity in the MVB variant in combination with the formation of multiscale microstructures, give rise to an ultralow κ_L compared with covalently bonded GeSe. Consequently, a maximum $zT \sim 0.9$ at 773 K is attained for the rhombohedral $Ge_{0.8}Pb_{0.2}Se(CdTe)_{0.25}$. These results emphasize the crucial role of the distinctive two-step phase manipulation strategy driven by stepwise tailoring chemical bonds in improving the zT values for a wide range of low-symmetry TE materials.

RESULTS AND DISCUSSION

The first step of this study aims to obtain higher-symmetric rhombohedral GeSe with enhanced valley degeneracy via CdTe alloying. Accordingly, we synthesized GeSe(CdTe)$_x$ ($0 \leq x \leq 0.30$) samples and analyzed the products obtained using powder X-ray diffraction (XRD) patterns. Figure 2A displays the room temperature XRD results, alongside the standard XRD patterns of orthorhombic (Pnma) and rhombohedral GeSe (R3m) for comparison. For the sample with $x = 0$, all diffraction peaks can be indexed to a typical orthorhombic structure.[35] Upon CdTe alloying ($x = 0.10$), a small amount of rhombohedral phase emerges within the orthorhombic matrix. When x exceeds 0.15, the prevailing crystal structure of GeSe(CdTe)$_x$ transforms from an orthorhombic to a rhombohedral phase. This is evidenced by the gradual merging of three XRD peaks between 30° and 33° into a single peak and the emergence of distinct double peaks between 44° and 46°. Nevertheless, when x ranges from 0.10–0.30, the distance between the double peaks near 44°–46° remains virtually constant. This suggests that CdTe alloying cannot further effectively tailor the lattice constant of the rhombohedral phase.

The second step of the phase manipulation aims at fine-tuning the lattice constant of rhombohedral GeSe. We additionally incorporate Pb into the sample with $x = 0.25$ and obtain the nominal samples of $Ge_{1-y}Pb_ySe(CdTe)_{0.25}$ ($0 \leq y \leq 0.30$). The inclusion of Pb has two effects on the phase structure: (1) further suppressing the residual orthorhombic phase and (2) significantly reducing the distance between the double peaks near 44°–46°, bringing the interaxial angle (θ) closer to 90°. This phenomenon is advantageous for facilitating the convergence of multivalence bands and thereby increasing the N_V of rhombohedral GeSe,[27,28] as will be discussed subsequently.

Additionally, the incorporation of CdTe ($x = 0.05$) immediately promotes the *in situ* generation of CdSe impurity phase, attributable to the low solubility limit of dopants in orthorhombic GeSe.[48] The electronegativity difference between Cd and Se (0.86) is greater than that of Cd and Te (0.41). Thus, Cd is more inclined to bond with Se than Te. As a result, scanning electron microscopy (SEM) and energy dispersive X-ray spectroscopy (EDS) analyses have revealed the presence of trace amounts of CdSe impurity phases, ranging in size from submicron to micron scale (Figures S1 and S2, Supporting Information).

To more accurately illustrate the two-step phase manipulation achieved through progressively CdTe and Pb co-alloying, we calculate the phase ratios and lattice parameters of all the samples, as plotted in Figures 2B–2E. The proportions of both rhombohedral GeSe phase and micron-sized CdSe precipitations gradually rise with increasing CdTe content (Figure 2B). For example, in the $x = 0.25$ sample, the percentage of orthorhombic phase significantly descends to 10%, while the percentage of rhombohedral GeSe and micron-scale CdSe precipitates ascends to 68% and 22%, respectively. After Pb substitution, the percentage of the rhombohedral phase increases further. Intriguingly, the content of micron-scale CdSe precipitates substantially declines, possibly attributable to the enhanced solubility of the dopant in rhombohedral GeSe compared with its orthorhombic variant.[47] Specifically, the percentage of micron-scale CdSe precipitates ascends from a baseline of 0 wt % in binary GeSe to 22 wt % for the $x = 0.25$ sample, and then decreases to 9 wt % for the $y = 0.30$ sample. This results in a ratio of rhombohedral GeSe to orthorhombic GeSe and micron-scale CdSe of 84:7:9 for the $y = 0.30$ sample.

As depicted in Figure 2C, the lattice parameters *a*, *b*, and *c* of both orthorhombic and rhombohedral GeSe increase upon CdTe and Pb co-alloying, which

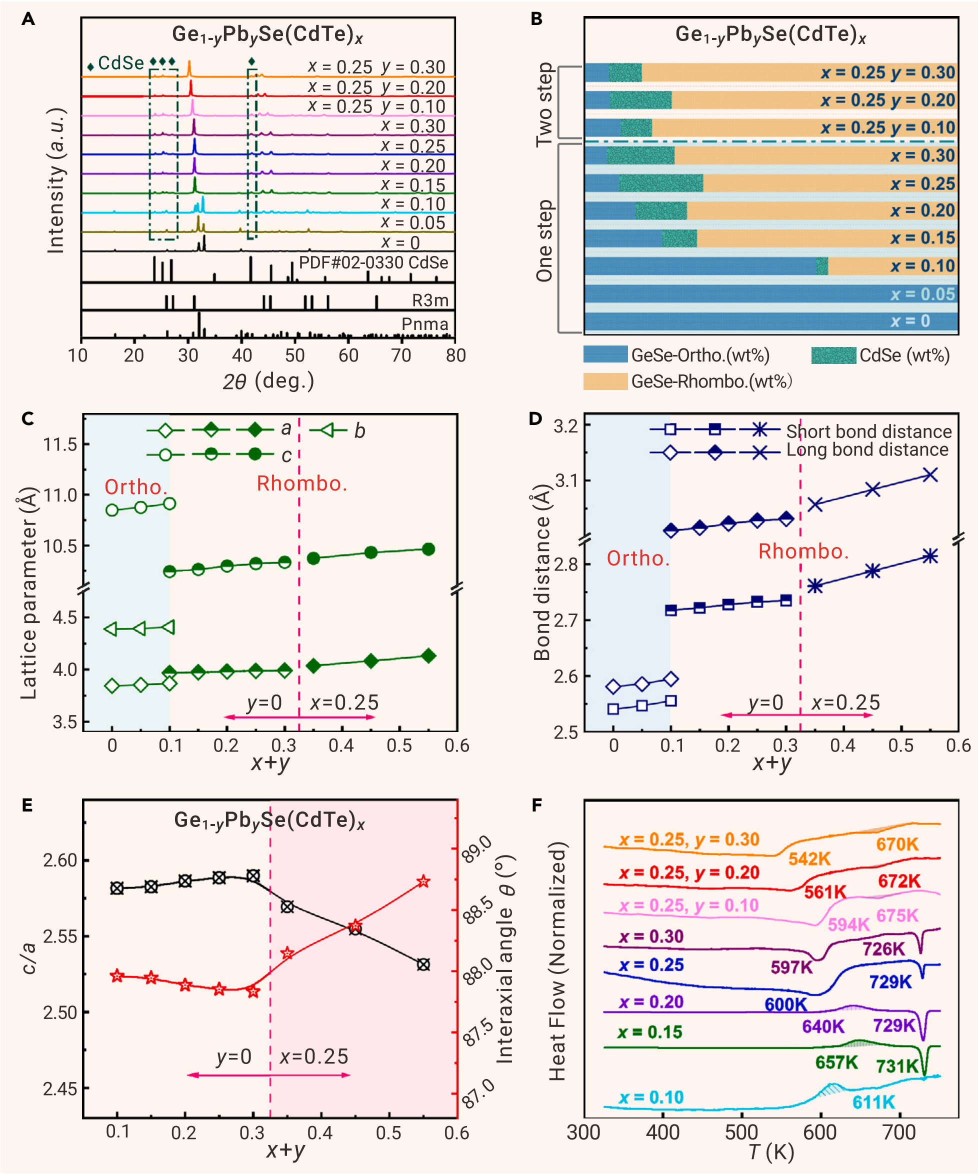

Figure 2. Examine the phases of as-prepared samples (A) Room temperature powder XRD patterns of $Ge_{1\text{-}y}Pb_ySe(CdTe)_x$ samples. The calculated (B) phase proportion; (C) lattice parameters *a*, *b*, *c*; (D) bond distances; and (E) the ratio of *c*/*a* and bond angles *θ* of $Ge_{1\text{-}y}Pb_ySe(CdTe)_x$ samples. (F) The DSC curves and the determined phase transition temperatures of representative $Ge_{1\text{-}y}Pb_ySe(CdTe)_x$ samples.

is attributed to the larger ionic radii of Cd (95 p.m.)/Pb (119 p.m.) and Te (221 p.m.) compared with those of Ge (73 p.m.) and Se (198 p.m.), respectively. Moreover, rhombohedral GeSe exhibits longer bond lengths than orthorhombic GeSe, suggesting weaker chemical bonds for the former (Figure 2D). This results in a lower sound velocity (v_m) and hence a reduced κ_L in thermoelectrics.[33,35] The ratio of *c*/*a* and the interaxial angle (*θ*), which provides a comprehensive assessment of the PD degree in rhombohedral GeSe,[21] remains nearly constant when *x* ranges from 0.10 to 0.30. Conversely, the value of *c*/*a* declines from 2.59 to 2.53 while the *θ* rises from 87.9° to 88.7° as the Pb content *y* increases from 0 to 0.3, signifying that Pb replacement can effectively reduce the PD.

We conducted differential scanning calorimetry (DSC) to cross-check the phase evolution upon CdTe-Pb co-alloying (Figure 2F). As for the samples with x = 0.10 to 0.20, a weak exothermic peak was detected, signaling an adverse transformation from the metastable rhombohedral phase to the stable orthorhombic or hexagonal phase (additional details are provided in the supplemental information).[21] For the $x \geq 0.25$ samples and *y* series, no detectable exothermic peaks were observed in the DSC curves. Instead, both of these samples showed two endothermic peaks, which were related to the rhombohedral-cubic phase transition and the orthorhombic-cubic phase transition, respectively.[21] In comparison with x = 0.25 and 0.30 samples, the tiny area of the second endothermic peak for the *y* series unraveled that Pb alloying greatly reduced the percentage of the orthorhombic phase, which is in line with the XRD results. More importantly, the rhombohedral-cubic phase transition temperature corresponding to the first endothermic peak gradually declined from 600 K to 542 K as *y* increased from 0 to 0.3, further indicating a moderate suppression of the PD of rhombohedral GeSe.

To examine the impact of the crystal structures and microstructures on the TE properties obtained, we employed transmission electron microscopy (TEM) characterizations to analyze the $Ge_{0.8}Pb_{0.2}Se(CdTe)_{0.25}$ sample as an example. The results are displayed in Figure 3. TEM images in Figures 3A–3C reveal high-density herringbone domain structures. Due to the phase transition from cubic to rhombohedral structures with symmetry reduction, such ferroelectric domains along the <111> directions emerge to alleviate stress.[50] In comparison with the typical ferroelectric domains with a width of approximately 100 nm in GeTe,[51] our sample demonstrates a much narrower ferroelectric domain, which is only 15–35 nm in width (Figure 3B). These ferroelectric domains can effectively scatter phonons,[51] which partly explains the low κ_L obtained in our sample.

The high-resolution TEM (HRTEM) image in Figure 3D, taken from the framed area in Figure 3A, displays well-defined atomic arrangements, suggesting high-quality crystallinity. The corresponding fast Fourier transform (FFT) in the inset of Figure 3D can be indexed to the rhombohedral GeSe along the [100] zone axis. The intensity line profiles along (003) and (021) planes (Figures 3E and 3F) and the displayed atom arrangements by the zoom-in HRTEM image (Figure 3G) agree with the corresponding atomic model (Figure 3H). This further substantiates the formation of metavalently bonded rhombohedral GeSe.

We observed submicron-scale CdSe secondary phases, which may be attributed to the limited solubility of Cd in GeSe (Figure 3I), agreeing with the XRD and SEM results. Figure 3J is an HRTEM image showing three nanoscale particles, designated as “a, b, and c.” The FFT images (Figure 3K) indicate that a and b can be indexed to GeSe while c to CdSe. These high-angle phase boundaries between GeSe and CdSe can scatter low-frequency phonons due to interfacial acoustic mismatch.

To unveil the driving force of the structural transition of GeSe from orthorhombic to rhombohedral by alloying with CdTe and Pb, atom probe tomography (APT)[30] characterizations were carried out on $GeSe(CdTe)_{0.25}$ and $Ge_{0.8}Pb_{0.2}Se(CdTe)_{0.25}$ samples. Figure 4A shows the elemental distribution of sample $GeSe(CdTe)_{0.25}$, where a grain boundary (GB) is indicated by arrows. The corresponding linear composition profile across the GB in Figure 4B displays slightly different compositions in the abutting two grains. The content of Te varies between 12.5 at% and 20 at% in different grains, implying a large tolerance of composition in the rhombohedral GeSe phase.[35] This high content of Te is enough to increase the degree of *p*-orbital overlap, which enables a decreased degree of Peierls distortion as well as the chemical bonding transition from covalent bonding to metavalent bonding.[35] The MVB mechanism is verified by

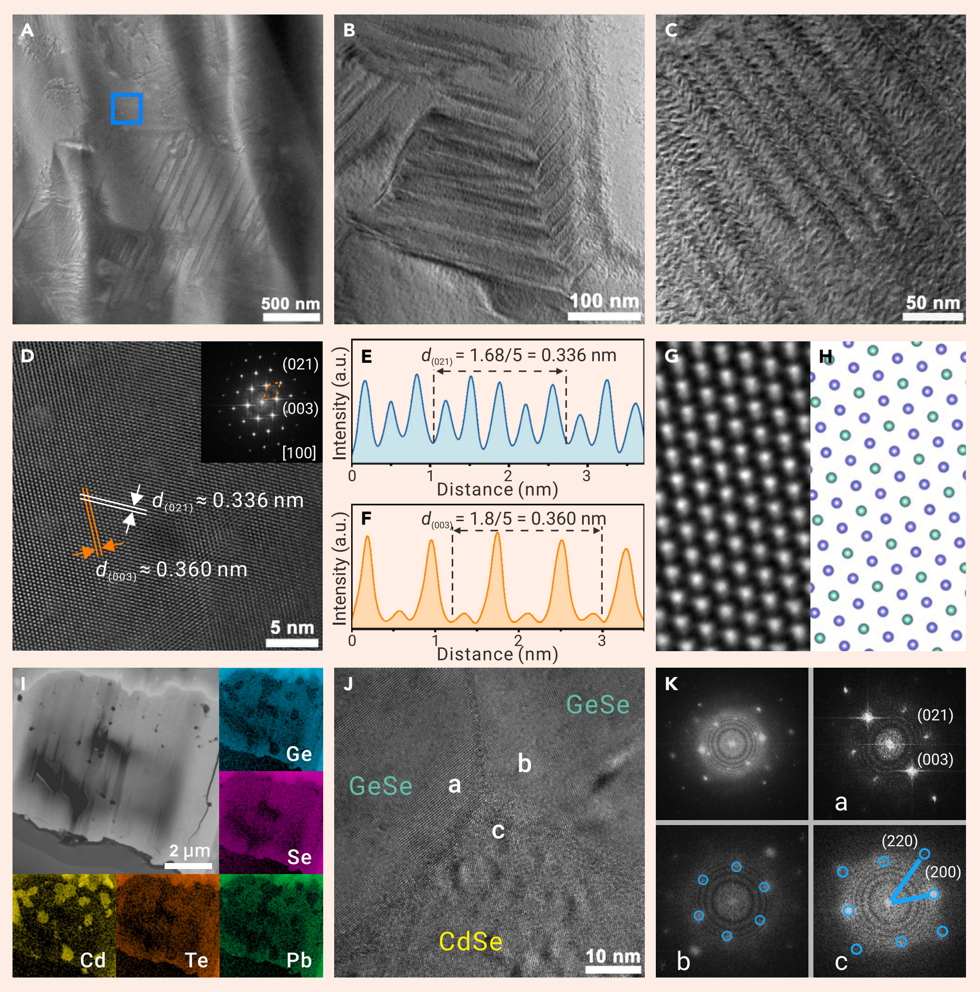

Figure 3. Structural characterization by transmission electron microscope (TEM) (A) The low-resolution image of the $Ge_{0.8}Pb_{0.2}Se(CdTe)_{0.25}$. (B and C) The structures of domains for different scales. (D) The high-resolution image collected from the blue box in (A), showing the atomic arrangement. The fast Fourier transform (FFT) of (D) displays the diffraction pattern of rhombohedral GeSe along the [100] direction (inset). (E and F) The corresponding intensity line profile alone (003) and (021) planes marked in D. (G) A close-up of D showing the arrays of atoms and (H) the corresponding atomic model of the rhombohedral phase. (I) TEM image and energy dispersive spectrum (EDS) mapping of the elemental Ge, Se, Cd, Pb, and Te, revealing the existence of CdSe second phases. (J) The high-resolution image showing the clear high-angle boundaries. (K) FFT analysis of (J) as well as the fraction of a, b, and c, indicating the phase boundary between GeSe and CdSe.

the high "probability of multiple events (PME)" observed in APT measurements, as shown in Figure 4C. PME describes the probability of dislodging more than one ion by breaking the chemical bonds in a successful laser pulse.[52,53] This high PME value is a hallmark of MVB compounds.[52,54] Note that the PME value drops at the GB due to the local collapse of MVB, which can impact the electron and phonon scattering strength at the GB.[55–57] This high PME value and MVB mechanism are in contrast to that of the pristine GeSe, which shows low PME and covalent bonding. Accordingly, the content of Te and other dopants in the covalent GeSe phase is much lower. We also observed the CdSe second phase with a low PME value in the sample $GeSe(CdTe)_{0.25}$, corroborating the iono-covalent bonding nature of CdSe, as presented in Figure S3, supporting information. The precipitation of CdSe will not impact the chemical bonding mechanism of the matrix as proved by the PME value of the matrix in Figure 4C. Note that two phases with different chemical bonding mechanisms are often immiscible.[58] Further alloying with Pb does not change the chemical bonding mechanism but modifies the local structural distortions as demonstrated by XRD results.

Figure 4D shows a homogeneous distribution of all constituent elements in the matrix of the sample $Ge_{0.8}Pb_{0.2}Se(CdTe)_{0.25}$, which can also be demonstrated in the linear composition profile in Figure 4E. The concentration of each element is very close to the nominal stoichiometry except for Cd and Se. This indicates that CdSe second phases should still exist in the Pb-alloyed samples, as has also been observed by TEM (Figure 3I). However, the CdSe precipitates are not included in the probed volume of APT measurements due to the limited field of view of APT (about 100 nm in diameter and 500 nm in length depending on the material). Nevertheless, due to the increased volume fraction of rhombohedral GeSe (Figure 2), the total number density of CdSe precipitates should decrease in the Pb-alloyed sample due to the much higher solubility of Cd in the rhombohedral phase than that in the pristine orthorhombic GeSe. The PME map in Figure 4F supports the MVB mechanism in the Pb-alloyed sample. Here, we demonstrate that the phase transition of GeSe from orthorhombic to rhombohedral by alloying with CdTe is accompanied by a chemical bonding transition from covalent to metavalent. This bonding transition will lead to a significant change in the electronic band structures and lattice vibration properties. Based on this MVB matrix, a very high content of Pb can be introduced into the lattice to further modify the degree of Peierls distortion and the concomitant transport properties, as is discussed in detail below.

To explore the impact of chemical bond-driven two-step phase manipulation on band structures, we performed first-principles calculations (DFT). Calculated band structures of orthorhombic and rhombohedral GeSe, CdTe-alloyed rhombohedral GeSe, and CdTe-Pb co-alloyed rhombohedral GeSe are depicted in Figures 5 and S4, supporting information. The one-step phase manipulation, i.e., elevating the crystal symmetry by substantially reducing the PD,[35] enhances the N_V of GeSe. In the orthorhombic phase, the valence band maximum (VB_1) is situated along the Γ-Z direction with an N_V of 2, while an extra valence band edge (VB_2) is positioned at the Γ point with an N_V of 1 (Figures 5A and 5C). VB_1 and VB_2 are separated by a small energy gap (ΔE) of 0.12 eV. As can be seen, orthorhombic GeSe has a low N_V. Besides, it is challenging to involve VB_2 in carrier transport. Theoretically, if the n_H of orthorhombic GeSe could be increased to 5×10^{19} cm^{-3}, both VB_1 and VB_2 could contribute to the carrier transport, resulting in an overall N_V of 3. However, the strong iono-covalent bonding in orthorhombic GeSe renders chemical doping exceedingly challenging.[48] Ag is the most effective acceptor dopant for orthorhombic GeSe, but it can only elevate the n_H to 10^{18} cm^{-3},[48] which is insufficient to activate VB_2 contribution. Favorably, rhombohedral GeSe has a much higher N_V. Specifically, the VB_1 is located at the L point with an N_V of 3, and the VB_2 is along the T-H direction with an N_V of 6 (refer to the calculated band structure and Fermi surface in Figures 5B and 5D). Therefore, by attaining an appropriate doping level, the N_V of rhombohedral GeSe can be increased to 9, far surpassing that of orthorhombic GeSe (N_V = 2).

Furthermore, the chemical bonding change associated with the phase transition contributes to additional improvements in electrical properties. First, the calculated E_g of rhombohedral GeSe (0.43 eV) is significantly lower than that of orthorhombic GeSe (0.76 eV), adhering to the 6–10 k_BT_o rule, where k_B is the Boltzmann constant and T_o is the operating temperature.[9] In general, the half-filled electronic energy band, which is the essence of MVB, should lead to a metallic ground state. Yet, this configuration is unstable against either a small Peierls distortion or a moderate charge transfer.[59] Both processes open the bandgap, turning these chalcogenides into narrow-bandgap semiconductors. This explains the narrowed bandgap from orthorhombic to rhombohedral GeSe due to the suppressed Peierls distortion. This appropriate E_g preserves high σ without pronounced adverse bipolar effects. Second, the band structure

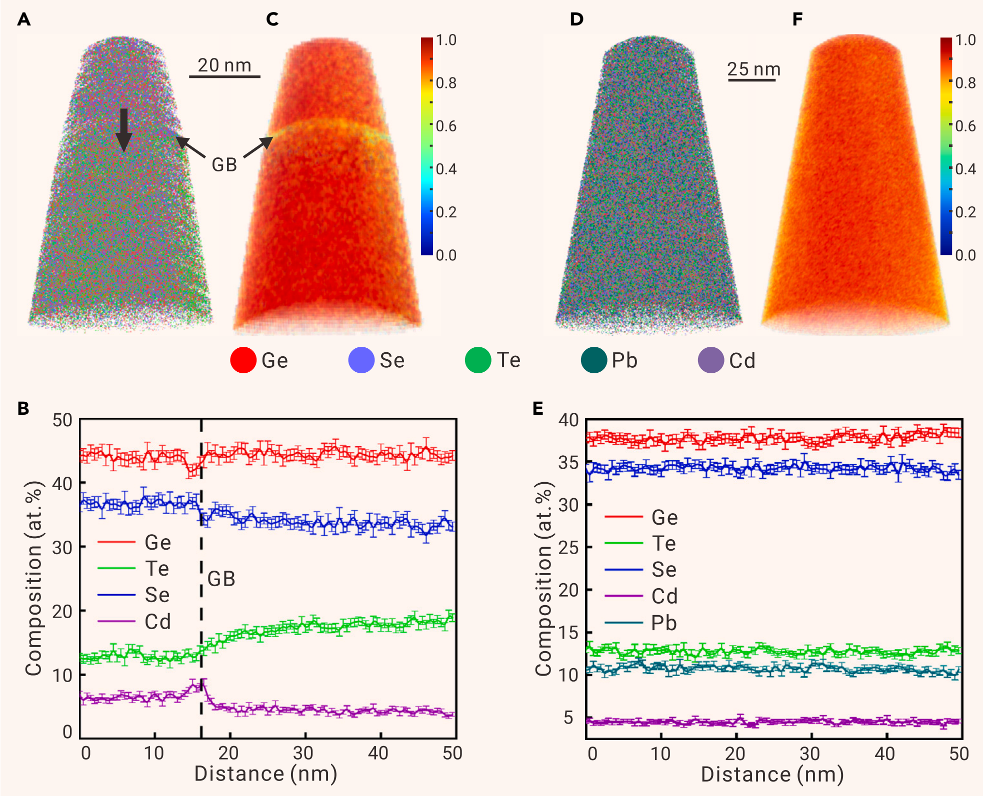

Figure 4. APT characterization results of $GeSe(CdTe)_{0.25}$ and $Ge_{0.8}Pb_{0.2}Se(CdTe)_{0.25}$ samples (A) 3D distribution of elements Ge, Se, Te, and Cd, where a GB is indicated by an arrow. (B) Composition profile across the GB along the arrow direction in (A). (C) 3D PME map demonstrating the abnormal bond-breaking behavior indicative of the MVB mechanism. The local decrease in PME at the GB indicates the breakdown of MVB there. (D) 3D distribution of elements Ge, Se, Te, Pb, and Cd. No obvious segregation and clusters are found. (E) Composition profile along the vertical direction calculated in a cuboid region of interest. A high solubility of Pb close to its nominal value is obtained, while the content of Cd is lower than its nominal one, demonstrating the presence of CdSe precipitates as observed in TEM. (F) 3D PME map verifies the MVB mechanism in the Pb-alloyed sample.

curvature drastically diminishes from the orthorhombic phase to the rhombohedral phase due to the shrinkage of the bandgap, suggesting a reduced m_b^*, which favors a high μ_H. Last, rhombohedral GeSe containing weaker metavalent bonds as verified by the small bond order (1/2) generates more cation vacancies compared with orthorhombic GeSe with strong covalent bonding, substantially increasing the n_H. This, in turn, promotes the solubility of dopants in metavalently bonded GeSe, granting it superior tunable TE performance.

Although the one-step phase manipulation effectively increases N_V, the ΔE between VB_1 and VB_2 in rhombohedral GeSe remains at 0.24 eV, which is higher than that observed in cubic PbTe (0.15 eV)[60] and rhombohedral GeTe (0.15 eV).[12] Consequently, the subsequent phase manipulation further reduces the PD and encourages the convergence of the valence bands. Evidently, the ΔE initially slightly decreased from 0.24 eV for binary rhombohedral GeSe to 0.19 eV (Figure 5D) for CdTe alloyed sample (Figure 5E), and subsequently experienced a substantial reduction to 0.10 eV for CdTe-Pb co-alloyed one (Figure 5F).

To elucidate the impact of two-step phase manipulation on the electrical properties, we measured the room temperature n_H and μ_H for all $Ge_{1-y}Pb_ySe(CdTe)_x$ samples (Figure 6). In comparison with orthorhombic GeSe, co-alloying with CdTe and Pb results in a remarkable increase in n_H, which originates from the rhombohedral structure with a lower formation energy of Ge vacancies (Figure 6A) due to the weak metavalent chemical bonds.[9] Typically, the room temperature n_H dramatically rises from 1.2×10^{16} cm^{-3} for binary GeSe to 4.3×10^{20} cm^{-3} for $x = 0.20$ sample, representing a four-order of magnitude enhancement. Notably, previous studies have reported that n_H values for $GeSe(AgSbTe_2)_x$,[41] $GeSe(AgSbSe_2)_x$,[39] and $(GeSe)_{1-x}(Sb_2Te_3)_x$[45] fall rapidly with increasing x after forming the exclusive rhombohedral (or cubic) phase. This is mainly because the rhombohedral or cubic GeSe alloys can be largely mixed with Ag-V-VI$_2$ and Sb_2Te_3 due to the same MVB mechanism utilized by these phases.[58] The increased content of Sb and Bi plays a role as donor dopants that decrease the hole concentration. In contrast, our findings indicate that n_H remains relatively constant as x increases. This observation can be ascribed to the combined effects of the increasing ratio of the rhombohedral to orthorhombic phase, which successively elevates the Ge vacancy concentration, and the increased overall size of cations after Cd alloying, which marginally suppresses the formation of Ge vacancies.[9] Nevertheless, the n_H of 4.3×10^{20} cm^{-3} exceeds the optimal level.[39] To resolve this issue, extra Pb atoms with a larger radius were utilized to replace Ge, thereby alleviating the excessive Ge vacancies and reducing the n_H.[61] In particular, as y increases from 0 to 0.3, the room temperature n_H progressively decreases from 4.3×10^{20} cm^{-3} to 7.7×10^{19} cm^{-3}.

The observed monotonic increase in μ_H for $GeSe(CdTe)_x$ can be attributed to the increased ratio of the rhombohedral phase upon CdTe alloying, which possesses a lighter m_b^* due to the smaller degree of PD and thus a narrower bandgap compared with that of orthorhombic phase (Figure 6B).[9] Here, we noticed a simultaneous increase of the charge carrier concentration and mobility in the rhombohedral phase due to the unique metavalent bonding mechanism. Conversely, the additional Pb alloying results in a slight decline in μ_H due to the point defect scattering on charge carriers. Typically, the room temperature μ_H experiences a significant increase from 1.3 cm^{2}V^{-1}s^{-1} for GeSe to 14.9 cm^{2}V^{-1}s^{-1} for the $x = 0.25$ sample, and subsequently drops slightly to 10.3 cm^{2}V^{-1}s^{-1} for the $y = 0.2$ sample. As shown in Figure 6C, the electrical conductivity σ experiences a marked rise with CdTe alloying, primarily due to the concurrent increase in n_H and μ_H. Furthermore, the incorporation of Pb results in a moderate reduction of σ because of the simultaneous decrease in n_H and μ_H. For example, the room temperature σ notably increases from 0.26 Sm^{-1} for GeSe to 1.0×10^5 Sm^{-1} for the $x = 0.25$ sample, and then diminishes to 1.80×10^4 Sm^{-1} for the $y = 0.2$ sample.

In contrast to the variation of σ, α exhibits a sharp decline with increasing CdTe content (Figure 6D). This behavior can be attributed to the four-order of magnitude increase in n_H. Subsequently, the substitution of Ge by Pb mitigates the excessive n_H and substantially enhances α across the entire temperature range. Typically, the room temperature α rapidly diminishes from 775 μVK^{-1} for GeSe to 70 μVK^{-1} for the $x = 0.25$ sample, followed by a remarkable increase to 233 μVK^{-1} for the $y = 0.30$ sample.

Apart from n_H, α strongly hinges on the N_V and hence m^*. Based on the single parabolic band (SPB) model (details can be found in the supplemental information), the relationship between α and n_H at room temperature, known as the Pisarenko curve,[62] is calculated to emphasize the decisive role of the two-step phase modulation on m^* (Figure 6E). First, orthorhombic GeSe owns a very small $m^* \sim 0.72\, m_0$ due to the low N_V, which agrees with the literature data.[46,48] Second, we observe that CdTe alloying modifies the crystal symmetry of GeSe from orthorhombic to rhombohedral by markedly suppressing the PD. This alteration increases the valley degeneracy, raising m^* from 0.72 m_0 to 2.0 m_0. Moreover, Pb alloying slightly reduces the PD within rhombohedral GeSe, promoting the convergence of valence bands and further boosting m^* to 3.5 m_0. As a consequence, the α of the $y = 0.20$ sample is 173 μVK^{-1} at 300 K, reaches a peak value of 250 μVK^{-1} at 473 K, and maintains 225 μVK^{-1} at 773 K. These findings underscore the efficacy of our two-step phase manipulation strategy in tailoring band structures in low-symmetry TE materials.

The synergy of excellent σ and decent α through two-step phase manipulation contributes to high PF throughout the temperature range for our GeSe-based alloys (Figure 6F). The dramatic increase in PF after CdTe alloying primarily originates from the simultaneous increase in n_H, μ_H, and m^*. Especially, the PF

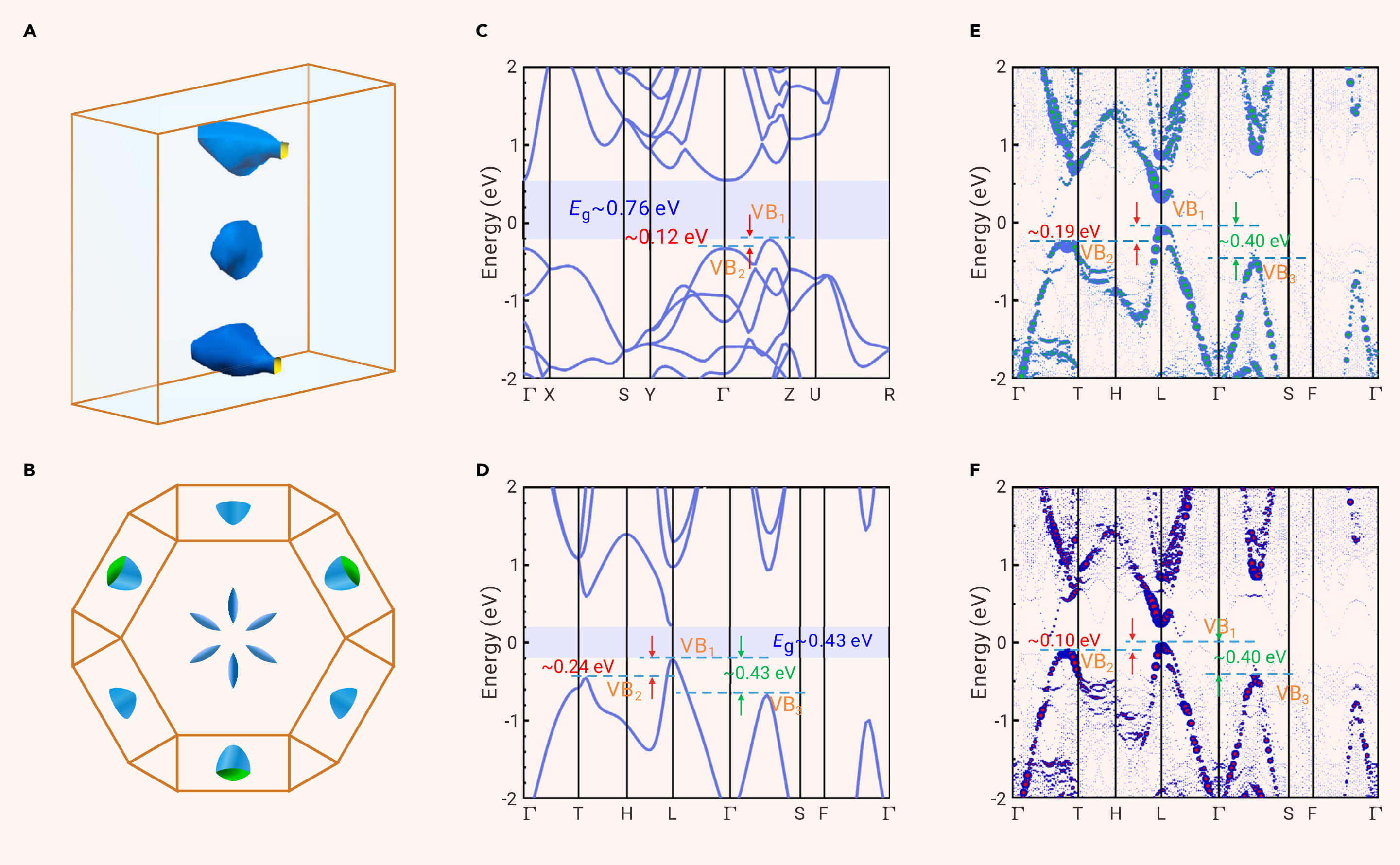

Figure 5. Calculated electronic band structures The Fermi energy in the first Brillouin zone for (A) orthorhombic and (B) rhombohedral GeSe. Electronic band structures for (C) orthorhombic $Ge_{27}Se_{27}$, (D) rhombohedral $Ge_{27}Se_{27}$, (E) rhombohedral $Ge_{26}CdSe_{22}Te_5$, and (F) rhombohedral $Ge_{21}CdPb_4Se_{22}Te_5$.

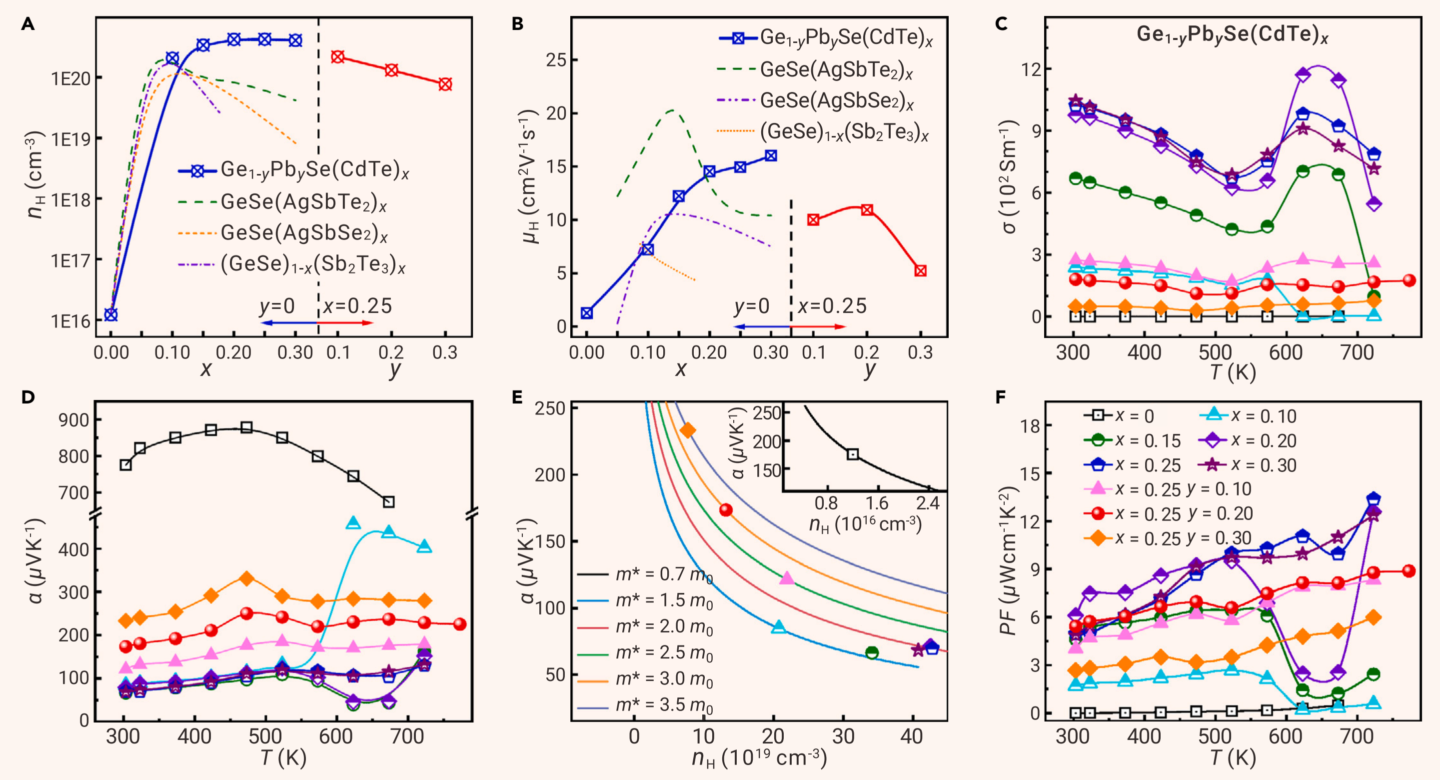

Figure 6. Electrical transport properties The room temperature (A) carrier concentration (n_H) and (B) carrier mobility (μ_H) of $Ge_{1-y}Pb_ySe(CdTe)_x$ samples ($0 \leq x \leq 0.30$, $0.10 \leq y \leq 0.30$) together with literature data.[39,41,45] Temperature dependence of (C) electrical conductivity (σ), (D) Seebeck coefficient (α), and (F) power factor (PF) of $Ge_{1-y}Pb_ySe(CdTe)_x$ samples. (E) The calculated Pisarenko curves at room temperature for $Ge_{1-y}Pb_ySe(CdTe)_x$ samples based on the SPB model.

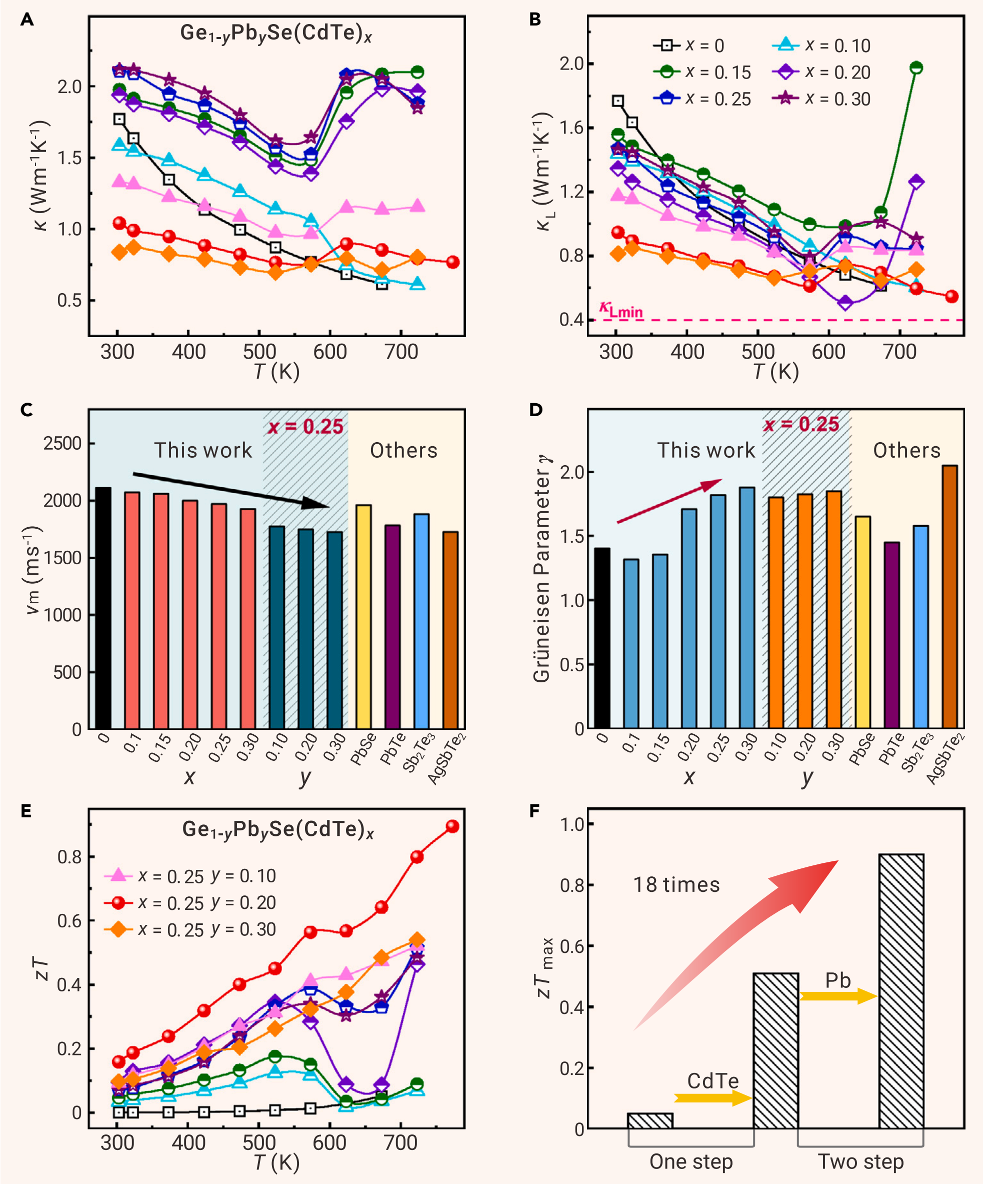

Figure 7. Thermal transport properties and zT values Temperature dependence of (A) thermal conductivity (κ), (B) lattice thermal conductivity (κ_L), and (E) zT values. (C) The mean sound velocity (v_m), and (D) Grüneisen parameter (γ) at room temperature for our GeSe-based alloys together with literature data.[68–70] (F) The advance of average zT_{ave} values for the $Ge_{1-y}Pb_ySe(CdTe)_x$ samples in this work.

of the $x = 0.25$ sample reaches 1.3×10^{-3} $Wm^{-1}K^{-2}$ at 723 K, which is comparable to most advanced GeSe-based alloys.[9,21,39,41–45] Even though the orbital degeneracy and m^* are increased by further Pb alloying, the PF at high temperatures is slightly decreased. This is mainly because of the reduction in μ_H induced by the strong alloy scattering upon Pb alloying. Nevertheless, the reduced μ_H will be compensated for by the enhanced phonon scattering that decreases the κ_L. This will result in a net increase in the final zT value, which is discussed below. In addition, the abrupt decline in the PF for $x = 0.10–0.20$ samples observed at approximately 650 K correlates with an undesirable transition from the metastable rhombohedral phase to either the stable orthorhombic or hexagonal phase.[21] Further insights into this correlation and the underlying mechanisms are detailed in the supplemental information.

The two-step phase manipulation also exerts a considerable impact on κ (Figure 7A). κ first increases with CdTe content, except for the $x = 0.10$ sample, and then significantly declines after further Pb alloying. Specifically, the room temperature κ climbs from 1.7 $Wm^{-1}K^{-1}$ for pristine GeSe to 2.1 $Wm^{-1}K^{-1}$ for the $x = 0.25$ sample, and subsequently descends to 0.8 $Wm^{-1}K^{-1}$ for the $y = 0.30$ sample.

The high κ_L of binary GeSe, obtained by excluding κ_e from κ, is effectively restrained due to the two-step phase manipulation, as depicted in Figures 7B and S5, supporting information. The κ - κ_e for all samples demonstrates an initial descent with increasing temperature, signifying the negligible impact of the bipolar effect near room temperature. This allows us to confidently discuss the effect of two-step phase manipulation on room temperature κ_L, without the need to account for the bipolar effect. The room temperature κ_L initially drops from 1.8 $Wm^{-1}K^{-1}$ for GeSe to 1.3 $Wm^{-1}K^{-1}$ for the $x = 0.20$ sample. However, when $x > 0.20$, the κ_L experiences slight growth, attributable to the significantly increased number and size of the micron-scale CdSe secondary phases with intrinsically higher κ_L.[63] Interestingly, the subsequent Pb alloying promotes the dissolution of excessive micron-scale CdSe secondary phases and facilitates the atomic-scale $Pb_{Ge}^{\times}$, leading to a significant reduction in κ_L again. Especially, a minimum $\kappa_L \sim 0.55$ $Wm^{-1}K^{-1}$ at 773 K is attained for $Ge_{0.80}Pb_{0.20}Se(CdTe)_{0.25}$ sample, approaching the amorphous limit of GeSe (0.39 $Wm^{-1}K^{-1}$).[48] How does the two-step phase modulation suppress the κ_L? The answer lies in the fact that the progressively CdTe and Pb co-alloying allows for the rational design and integrated construction of multiscale microstructures, which encompass atomic-scale substitutions and Ge vacancies, nanoscale domains, as well as the dispersive micron-size CdSe precipitates. The formation of such multiscale microstructures can scatter broad wavelength phonons accumulatively.[64,65] Figure S6 in the supporting information depicts the impact of defects with varying scales on the κ_L, quantified through the Debye-Callaway model.[66]

In addition, the two-step phase manipulation also enables the precise modification of the phonon dispersion relation. On the one hand, both weak chemical bonds and heavy atoms contribute to the low sound velocity (v_m).[33] Orthorhombic GeSe is formed by strong covalent bonding.[35] In contrast, the rhombohedral GeSe is generated by weak metavalent bonding.[35] From Table S1, supporting information, it is evident that rhombohedral GeSe with metavalent bonding owns lower Young's modulus (E) and Debye temperature (θ_D), indicating weaker chemical bonding compared with orthorhombic GeSe utilizing covalent bonding. Coupled with the increased atomic masses upon the substitution of Cd and Pb on Ge sites and Te on Se sites, the room temperature v_m is substantially reduced from 2112 ms^{-1} for GeSe to 1726 ms^{-1} for the $y = 0.30$ sample (Figure 7C). The Grüneisen parameter (γ), which stands for the lattice anharmonicity,[33] increases from 1.4 for orthorhombic GeSe to 1.8 for rhombohedral samples because of the highly delocalized p-electrons in metavalent bonds (Figure 7D).[67] These delocalized p-electrons couple with transverse optical (TO) phonons, as well as the Peierls distortion is related to a lattice instability, which lowers the frequency of TO phonons, due to the high values of the Born effective charge in these MVB monochalcogenides. This increases the phase space for Umklapp phonon scattering processes and significantly reduces the κ_L.[67] Interestingly, the v_m and γ in our rhombohedral GeSe-based alloys are comparable to those in advanced metavalently bonded TE materials such as PbSe,[68] PbTe,[68] Sb_2Te_3,[69] and $AgSbTe_2$.[70]

The synergy of the beneficial outcomes of two-step phase modulation on band structure, phonon dispersion relation, and microstructure results in a remarkable enhancement of the zT value (Figure 7E). Notably, the peak zT of 0.90 at 773 K is attained for $Ge_{0.80}Pb_{0.20}Se(CdTe)_{0.25}$, representing an approximately 18-fold increase compared with the pristine orthorhombic GeSe with a maximum *zT* of 0.05 at 673 K (Figure 7F). While GeSe might display suboptimal TE performance in comparison with certain IV-VI counterparts, the overarching emphasis of our study is not on the material-specific properties, but on a pioneering two-step phase manipulation strategy grounded in progressive chemical bond tailoring. These results not only highlight the significant role of two-step phase manipulation in enhancing the figure of merit for low-symmetric materials but also suggest the potential of stepwise tailoring chemical bonds to expand the scope of TE materials research.

CONCLUSION

For low-symmetry compounds with limited band degeneracy, the conventional one-step phase manipulation strategy, relying solely on the valley or orbital degeneracy, proves insufficient to achieve a high density-of-states effective mass and, consequently, exceptional TE performance. In this work, we introduce a novel two-step phase manipulation strategy through sequential tailoring of chemical bonds in GeSe via CdTe and Pb co-alloying. The CdTe alloying promotes the transition of chemical bonding from covalent to metavalent by substantially suppressing the Peierls distortion, altering the crystal structure of GeSe from a low-symmetric orthorhombic phase to a medium-symmetric rhombohedral phase. This transition elevates the crystal symmetry, thereby enhancing the valley degeneracy. Subsequently, the incorporation of Pb further moderately reduces the Peierls distortion and the associated electronic band structures, leading to multivalence band convergence and a significant increase in density-of-states effective mass. Moreover, the metavalently bonded GeSe exhibits a lower formation energy for Ge vacancy, lighter band effective mass, stronger lattice anharmonicity, and reduced sound velocity. These characteristics yield a higher carrier concentration, improved carrier mobility, and restrained lattice thermal conductivity compared with its covalently bonded counterpart. As a result, rhombohedral Ge$_{0.8}$Pb$_{0.2}$Se(CdTe)$_{0.25}$ attains a maximum *zT* ~ 0.9 at 773 K, representing an 18-fold increase compared with the orthorhombic GeSe. These findings underscore the significant role of the two-step phase manipulation strategy, achieved through stepwise tailoring of chemical bonds, in enhancing the *zT* of numerous low-symmetric materials.

MATERIALS AND METHODS

See the supplemental information for detail.

REFERENCES

1. Xiao, C., Qin, X., Zhang, J., et al. (2012). High Thermoelectric and Reversible p-n-p Conduction Type Switching Integrated in Dimetal Chalcogenide. J. Am. Chem. Soc. ***134***, 18460–18466.
2. Chen, L.C., Chen, P.Q., Li, W.J., et al. (2019). Enhancement of thermoelectric performance across the topological phase transition in dense lead selenide. Nat. Mater. ***18***, 1321–1326.
3. Zhi, S., Li, J., Hu, L., et al. (2021). Medium Entropy-Enabled High Performance Cubic GeTe Thermoelectrics. Adv. Sci. ***8***, 2100220.
4. Zheng, Z., Su, X., Deng, R., et al. (2018). Rhombohedral to Cubic Conversion of GeTe via MnTe Alloying Leads to Ultralow Thermal Conductivity, Electronic Band Convergence, and High Thermoelectric Performance. J. Am. Chem. Soc. ***140***, 2673–2686.
5. Liu, Z., Sun, J., Mao, J., et al. (2018). Phase-transition temperature suppression to achieve cubic GeTe and high thermoelectric performance by Bi and Mn codoping. Proc. Natl. Acad. Sci. USA ***115***, 5332–5337.
6. Agne, M.T., Voorhees, P.W., and Snyder, G.J. (2019). Phase Transformation Contributions to Heat Capacity and Impact on Thermal Diffusivity, Thermal Conductivity, and Thermoelectric Performance. Adv. Mater. ***31***, e1902980.
7. Wang, S., Sun, Y., Yang, J., et al. (2016). High thermoelectric performance in Te-free (Bi,Sb) 2Se3via structural transition induced band convergence and chemical bond softening. Energy Environ. Sci. ***9***, 3436–3447.
8. Jiang, B., Qiu, P., Chen, H., et al. (2018). Entropy optimized phase transitions and improved thermoelectric performance in n-type liquid-like Ag9GaSe6 materials. Mater. Today Phys. ***5***, 20–28.
9. Li, X., Liang, Z., Li, J., et al. (2022). Crystal symmetry enables high thermoelectric performance of rhombohedral GeSe(MnCdTe2)x. Nano Energy ***100***, 107434.
10. Shi, X.L., Zou, J., and Chen, Z.G. (2020). Advanced Thermoelectric Design: From Materials and Structures to Devices. Chem. Rev. ***120***, 7399–7515.
11. Hu, H., Wang, Y., Fu, C., et al. (2022). Achieving metal-like malleability and ductility in Ag2Te1-xSx inorganic thermoelectric semiconductors with high mobility. Innovation ***3***, 100341.
12. Hong, M., Li, M., Wang, Y., et al. (2023). Advances in Versatile GeTe Thermoelectrics from Materials to Devices. Adv. Mater. ***35***, 2208272.
13. Yan, Q., and Kanatzidis, M.G. (2022). High-performance thermoelectrics and challenges for practical devices. Nat. Mater. ***21***, 503–513.
14. Sun, P., Kumar, K.R., Lyu, M., et al. (2021). Generic Seebeck effect from spin entropy. Innovation ***2***, 100101.
15. Qin, B., and Zhao, L. (2022). Carriers: the less, the faster. Mat. Lab ***1***, 220004.
16. He, Y., Day, T., Zhang, T., et al. (2014). High Thermoelectric Performance in Non-Toxic Earth-Abundant Copper Sulfide. Adv. Mater. ***26***, 3974–3978.
17. Zhu, H., Zhao, T., Zhang, B., et al. (2021). Entropy Engineered Cubic n-Type AgBiSe2 Alloy with High Thermoelectric Performance in Fully Extended Operating Temperature Range. Adv. Energy Mater. ***11***, 9.
18. Liang, Q., Yang, D., Xia, F., et al. (2021). Phase-Transformation-Induced Giant Deformation in Thermoelectric Ag2Se Semiconductor. Adv. Funct. Mater. ***31***, 7.
19. Chang, J.T., Wang, B., He, D.S., et al. (2019). Realizing High-Ranged Out-of-Plane ZTs in N-Type SnSe Crystals through Promoting Continuous Phase Transition. Inj. Epidemiol. ***6***, 10.
20. Guo, Z., Wu, G., Tan, X., et al. (2023). Enhanced Thermoelectric Performance in GeTe by Synergy of Midgap state and Band Convergence. Adv. Funct. Mater. ***33***, 2212421.
21. Wang, Z., Wu, H., Zhang, B., et al. (2022). Phase Modulation Enabled High Thermoelectric Performance in Polycrystalline GeSe0.75Te0.25. Adv. Funct. Mater. ***32***, 9.
22. Fu, C., Bai, S., Liu, Y., et al. (2015). Realizing high figure of merit in heavy-band p-type half-Heusler thermoelectric materials. Nat. Commun. ***6***, 8144.
23. Liu, R., Chen, H., Zhao, K., et al. (2017). Entropy as a Gene-Like Performance Indicator Promoting Thermoelectric Materials. Adv. Mater. ***29***, 1702712.
24. Hong, M., Chen, Z.G., Yang, L., et al. (2018). Realizing zT of 2.3 in Ge1-x-ySbxInyTe via Reducing the Phase-Transition Temperature and Introducing Resonant Energy Doping. Adv. Mater. ***30***, 8.
25. Zhang, J., Liu, R., Cheng, N., et al. (2014). High-Performance Pseudocubic Thermoelectric Materials from Non-cubic Chalcopyrite Compounds. Adv. Mater. ***26***, 3848–3853.
26. Hong, M., Lyv, W., Li, M., et al. (2020). Rashba Effect Maximizes Thermoelectric Performance of GeTe Derivatives. Joule ***4***, 2030–2043.
27. Li, J., Lv, S., Qiu, X., et al. (2018). Low-Symmetry Rhombohedral GeTe Thermoelectrics. Joule ***9***, 976–980.
28. Zhang, X., Bu, Z., Lin, S., et al. (2020). GeTe Thermoelectrics. Joule ***4***, 986–1003.
29. Tan, X., Zhang, F., Zhu, J., et al. (2023). High-Power Factor Enabled by Efficient Manipulation Interaxial Angle for Enhancing Thermoelectrics of GeTe-Cu2Te Alloys. ACS Appl. Mater. Interfaces ***15***, 9315–9323.
30. Wuttig, M., Schön, C.F., Lötfering, J., et al. (2023). Revisiting the nature of chemical bonding in chalcogenides to explain and design their properties. Adv. Mater. ***35***, 2208485.
31. Jiang, B., Wang, W., Liu, S., et al. (2022). High figure-of-merit and power generation in high-entropy GeTe-based thermoelectrics. Science ***377***, 208–213.
32. Su, L., Wang, D., Wang, S., et al. (2022). High thermoelectric performance realized through manipulating layered phonon-electron decoupling. Science ***375***, 1385–1389.
33. Yu, Y., Cagnoni, M., Cojocaru-Mirédin, O., et al. (2020). Chalcogenide Thermoelectrics Empowered by an Unconventional Bonding Mechanism. Adv. Funct. Mater. ***30***, 1904862.
34. Munirathnappa, A.K., Lee, H., and Chung, I. (2023). Recent advances in ultrahigh thermoelectric performance material. SnSe. Mat. Lab ***2***, 220056.
35. Cagnoni, M., Führen, D., and Wuttig, M. (2018). Thermoelectric Performance of IV–VI Compounds with Octahedral-Like Coordination: A Chemical-Bonding Perspective. Adv. Mater. ***30***, 1801787.
36. Schön, C.F., van Bergerem, S., Mattes, C., et al. (2022). Classification of properties and their relation to chemical bonding: Essential steps toward the inverse design of functional materials. Sci. Adv. ***8***, eade0828.
37. Wuttig, M., Deringer, V.L., Gonze, X., et al. (2018). Incipient metals: functional materials with a unique bonding mechanism. Adv. Mater. ***30***, 1803777.
38. Arora, R., Waghmare, U.V., and Rao, C.N.R. (2023). Metavalent bonding origins of unusual properties of group IV chalcogenides. Adv. Mater. ***35***, 2208724.
39. Huang, Z., Miller, S.A., Ge, B., et al. (2017). High Thermoelectric Performance of New Rhombohedral Phase of GeSe stabilized through Alloying with AgSbSe2. Angew. Chem., Int. Ed. Engl. ***56***, 14113–14118.
40. Roychowdhury, S., Ghosh, T., Arora, R., et al. (2018). Stabilizing n-Type Cubic GeSe by Entropy-Driven Alloying of AgBiSe2: Ultralow Thermal Conductivity and Promising Thermoelectric Performance. Angew. Chem., Int. Ed. Engl. ***57***, 15167–15171.
41. Yan, M., Tan, X., Huang, Z., et al. (2018). Synergetic optimization of electronic and thermal transport for high-performance thermoelectric GeSe–AgSbTe2 alloy. J. Mater. Chem. A ***6***, 8215–8220.
42. Wang, Z., Wu, H., Xi, M., et al. (2020). Structure-Dependent Thermoelectric Properties of GeSe1−xTex (0 ≤ x ≤ 0.5). ACS Appl. Mater. Interfaces ***12***, 41381–41389.
43. Sarkar, D., Ghosh, T., Roychowdhury, S., et al. (2020). Ferroelectric Instability Induced Ultralow Thermal Conductivity and High Thermoelectric Performance in Rhombohedral p-Type GeSe Crystal. J. Am. Chem. Soc. ***142***, 12237–12244.
44. Sarkar, D., Roychowdhury, S., Arora, R., et al. (2021). Metavalent Bonding in GeSe Leads to High Thermoelectric Performance. Angew. Chem., Int. Ed. Engl. ***60***, 10350–10358.
45. Yan, M., Geng, H., Jiang, P., et al. (2020). Glass-like electronic and thermal transport in crystalline cubic germanium selenide. J. Energy Chem. ***45***, 83–90.
46. Lyu, T., Li, X., Yang, Q., et al. (2022). Stepwise Ge vacancy manipulation enhances the thermoelectric performance of cubic GeSe. Chem. Eng. J. ***442***, 136332.
47. Duan, B., Zhang, Y., Yang, Q., et al. (2022). The Role of Cation Vacancies in GeSe: Stabilizing High-Symmetric Phase Structure and Enhancing Thermoelectric Performance. Adv. Energy Sustain. Res. ***3***, 2200124.
48. Zhang, X., Shen, J., Lin, S., et al. (2016). Thermoelectric properties of GeSe. J. Materiomics ***2***, 331–337.

49. Kooi, B.J., and Wuttig, M. (2020). Chalcogenides by design: Functionality through metavalent bonding and confinement. Adv. Mater. ***32***, 1908302.
50. Wu, D., Zhao, L.-D., Hao, S., et al. (2014). Origin of the high performance in GeTe-based thermoelectric materials upon Bi2Te3 doping. J. Am. Chem. Soc. ***136***, 11412–11419.
51. Zhong, J., Liang, G., Cheng, J., et al. (2023). Entropy engineering enhances the thermoelectric performance and microhardness of (GeTe)(1-x)(AgSb0.5Bi0.5Te2)(x). Sci. China Mater. ***66***, 696–706.
52. Zhu, M., Cojocaru-Mirédin, O., Mio, A.M., et al. (2018). Unique bond breaking in crystalline phase change materials and the quest for metavalent bonding. Adv. Mater. ***30***, 1706735.
53. Yu, Y., Cojocaru-Mirédin, O., and Wuttig, M. (2023). Atom Probe Tomography Advances Chalcogenide Phase-Change and Thermoelectric Materials. Phys. Status Solidi A.
54. Cheng, Y., Cojocaru-Mirédin, O., Keutgen, J., et al. (2019). Understanding the structure and properties of sesqui-chalcogenides (ie, V2VI3 or Pn2Ch3 (Pn= pnictogen, Ch= chalcogen) compounds) from a bonding perspective. Adv. Mater. ***31***, 1904316.
55. Rodenkirchen, C., Cagnoni, M., Jakobs, S., et al. (2020). Employing interfaces with metavalently bonded materials for phonon scattering and control of the thermal conductivity in TAGS-x thermoelectric materials. Adv. Funct. Mater. ***30***, 1910039.
56. Wu, R., Yu, Y., Jia, S., et al. (2023). Strong charge carrier scattering at grain boundaries of PbTe caused by the collapse of metavalent bonding. Nat. Commun. ***14***, 719.
57. Yu, Y., and Wuttig, M. (2023). Metavalent bonding impacts charge carrier transport across grain boundaries. Nano Res. Energy ***2***, 9120057.
58. Liu, Y., Zhang, X., Nan, P., et al. (2022). Improved Solubility in Metavalently Bonded Solid Leads to Band Alignment, Ultralow Thermal Conductivity, and High Thermoelectric Performance in SnTe. Adv. Funct. Mater. ***32***, 2209980.
59. Guarneri, L., Jakobs, S., von Hoegen, A., et al. (2021). Metavalent Bonding in Crystalline Solids: How Does It Collapse? Adv. Mater. ***33***, 2102356.
60. Zhao, L.D., Wu, H.J., Hao, S.Q., et al. (2013). All-scale hierarchical thermoelectrics: MgTe in PbTe facilitates valence band convergence and suppresses bipolar thermal transport for high performance. Energy Environ. Sci. ***6***, 3346.
61. Li, J., Hu, Q., He, S., et al. (2021). Enhancing Near-Room-Temperature GeTe Thermoelectrics through In/Pb Co-doping. ACS Appl. Mater. Interfaces ***13***, 37273–37279.
62. May, A.F., Toberer, E.S., Saramat, A., et al. (2009). Characterization and analysis of thermoelectric transport in n-type Ba8Ga16-xGe30+x. Phys. Rev. B ***80***, 125205.
63. Yang, J., Tang, H., Zhao, Y., et al. (2015). Thermal conductivity of zinc blende and wurtzite CdSe nanostructures. Nanoscale ***7***, 16071–16078.
64. Jiang, Y., Dong, J., Zhuang, H.-L., et al. (2022). Evolution of defect structures leading to high ZT in GeTe-based thermoelectric materials. Nat. Commun. ***13***, 6087.
65. Shu, R., Han, Z., Elsukova, A., et al. (2022). Solid-State Janus Nanoprecipitation Enables Amorphous-Like Heat Conduction in Crystalline Mg3Sb2-Based Thermoelectric Materials. Adv. Sci. ***9***, 2202594.
66. Callaway, J., and von Baeyer, H.C. (1960). Effect of Point Imperfections on Lattice Thermal Conductivity. Phys. Rev. ***120***, 1149–1154.
67. Lee, S., Esfarjani, K., Luo, T., et al. (2014). Resonant bonding leads to low lattice thermal conductivity. Nat. Commun. ***5***, 3525.
68. Zhang, Y., Ke, X., Chen, C., et al. (2009). Thermodynamic properties of PbTe, PbSe, and PbS: First-principles study. Phys. Rev. B ***80***, 024304.
69. Liu, X., Wang, D., Wu, H., et al. (2019). Intrinsically low thermal conductivity in BiSbSe3: a promising thermoelectric material with multiple conduction bands. Adv. Funct. Mater. ***29***, 1806558.
70. Morelli, D.T., Jovovic, V., and Heremans, J.P. (2008). Intrinsically minimal thermal conductivity in cubic I—V—VI2 semiconductors. Phys. Rev. Lett. ***101***, 035901.

ACKNOWLEDGMENTS

The work is supported by the National Natural Science Foundation of China (52071218), National Key R&D Program of China (2021YFB1507403), the Shenzhen University 2035 Program for Excellent Research (00000218), and the China Postdoctoral Science Foundation (2022M722170). Y.Y. and M.W. acknowledge support from the German Research Foundation (Deutsche Forchungsgemeinschaft, DFG) within project SFB917. Y.Y. acknowledges financial support under the Excellence Strategy of the Federal Government and the Länder within the ERS RWTH Start-Up grant (Grant No. StUpPD_392-21). The authors also appreciate the Instrumental Analysis Center of Shenzhen University.

AUTHOR CONTRIBUTIONS

Y.Y. and L.P.H. designed the project. Y.Y., M.H., and L.P.H. proposed valuable advice for revising the manuscript. W.Q.Y., Y.H.Z., T.L., W.B.H., N.X.H., and X.L. prepared the samples, characterized structures, and conducted properties measurements. C.H.Z., F.S.L., and M.W. analyzed the data formally. T.L. performed the TEM characterization and provided discussions. W.Q.Y., Y.Y., M.H., and L.P.H. wrote the original manuscript. M.W., Y.Y., and L.P.H. reviewed and edited articles. L.P.H. supervised the research work. All the authors reviewed and edited the manuscript.

DECLARATION OF INTERESTS

The authors declare no competing interests.

SUPPLEMENTAL INFORMATION

It can be found online at https://doi.org/10.1016/j.xinn.2023.100522.

LEAD CONTACT WEBSITE

https://cmse.szu.edu.cn/szdw1/jsml/clkxygcx/fjs/hlp.htm.